

Fabrication and testing of a miniature cylindrical ion trap mass spectrometer constructed from low temperature co-fired ceramics

A. Chaudhary^a, F.H.W. van Amerom^{a,*}, R.T. Short^a, S. Bhansali^b

^a Center for Ocean Technology, University of South Florida, 140 7th Av. S, St. Petersburg, FL 33701, USA

^b Department of Electrical Engineering, Nanomaterials and Nanomanufacturing Research Center, University of South Florida, 4202 E. Fowler Av., Tampa, FL 33620, USA

Received 20 October 2005; received in revised form 13 December 2005; accepted 13 December 2005

Available online 7 February 2006

Abstract

A novel technique for the fabrication of miniature cylindrical ion trap (CIT) mass spectrometers using a non-conductive substrate has been developed. This technique demonstrated the feasibility of batch fabricating accurate and low-cost CITs. A CIT ring electrode ($r_0 = 1.375$ mm) was fabricated using multiple layers of low temperature co-fired ceramics (LTCC) which were punched and then compressed in a ring-electrode die. Uniform compression was achieved, and cracking avoided, by tailoring the thickness of the LTCC stack. The stack was then fired at 850 °C to convert the LTCC into a ceramic ring. Areas to be metallized were patterned photolithographically after the ring was subjected to electroless plating. Stainless steel endplates were affixed to the ring electrode to complete the CIT. The prototype CIT was tested in the mass selective instability mode without axial modulation and produced mass spectra with a typical peak width of 1.8 m/z . Simulations of operation were also performed in ITSIM 5.0 after SIMION 7.0 was used to calculate the contribution of higher order multipoles to the nominally quadrupole potential inside the CIT. © 2005 Elsevier B.V. All rights reserved.

Keywords: Cylindrical ion trap; Metallized ceramic surface; Miniature; Photolithography; LTCC

1. Introduction

In situ sensors enable researchers to investigate real-time chemical dynamics in the environment, thereby greatly improving sampling densities and providing the capability for autonomous measurements in harsh environments [1,2]. For example, deployed sensors can be used to detect, quantify and trace harmful and toxic chemicals that have been released in populated areas [3]. Miniaturized mass spectrometers (MS) can be especially versatile and powerful as sensors for on-site identification and characterization of a wide variety of chemicals. Miniaturization is desirable for field-deployed mass spectrometers because of the corresponding reduction of electrical power consumption, simplification of vacuum systems, and the possibility for rapid parallel chemical analysis [4–8]. Recent

efforts in extreme miniaturization of mass spectrometers and their components have been stimulated by opportunities arising from micro-fabrication techniques and advances in materials sciences [8–11]. One team of researchers has focused on micro-fabrication of as many as a million micron-sized cylindrical ion trap (CIT) mass spectrometer arrays on silicon wafers [12]. An array-based approach for MS miniaturization can be useful to compensate for the reduced signal intensities that result from miniaturization of each mass spectrometer [13]. However, affordable batch fabrication of such arrays remains a challenge.

A key objective of this research was to simplify the fabrication and assembly of CITs using new materials and processes. Towards this objective, a CIT was made from low temperature co-fired ceramics (LTCC). LTCC are routinely used in semiconductor industry as a packaging material [14]. They have also been used for applications in physical MEMS [15] and RF (MEMS) devices [16]. LTCC have ceramic particles bound in an organic matrix, which results in the structure behaving as a flexible tape that can be shaped easily, e.g., with a knife. The LTCC sheets are laminated together under pressure to build up the

* Corresponding author. Tel.: +1 727 553 1283; fax: +1 727 553 3967.

E-mail addresses: ashishc@marine.usf.edu (A. Chaudhary), famerom@marine.usf.edu (F.H.W. van Amerom), tshort@marine.usf.edu (R.T. Short), bhansali@eng.usf.edu (S. Bhansali).

desired thickness of the unfired structure. Upon firing the organic compounds are volatilized and at 800 °C the glass in the ceramic reflows to impart rigidity to the structure. As the organics are volatilized, the structure shrinks. This shrinkage is a function of the lamination pressure (compaction) and firing cycle. This paper describes the use of LTCC to build CIT ring electrodes. For this work, a commercially available LTCC tape (DuPont 951™) was chosen. Test structures were made from LTCC to extract the optimum processing parameters (lamination pressure, method of stacking sheets, firing cycle) to obtain a stable structure devoid of cracks, and to determine the amount of shrinkage. The shrinkage data were used in the design of the ring-electrode punch, to ensure that the finished structure met design specifications. The fired ring was subjected to a novel three dimensional lithography process that enabled one-step metallization for completion of the ring electrode. To validate this fabrication method, the LTCC CIT was operated as a mass spectrometer to detect chloroform (CHCl₃) and perfluorotributylamine (PFTBA) calibration compound in separate experiments.

This paper describes the design and simulation of operation of the CIT followed by a detailed discussion of the fabrication process and assembly of the LTCC CIT. A description of the experimental setup is then followed by characterization of the performance of the CIT mass spectrometer.

2. Experimental

2.1. Design and simulations

Several research groups have invested considerable effort to optimize hyperbolic, cylindrical and hybrid ion trap geometries for operation as mass spectrometers [17–22]. Simulation of ion trap operation using programs such as ITSIM 5.0 [23], developed at Purdue University, can be very helpful in expediting the optimization of designs by obviating the need to physically construct multiple trap geometries. Simulations using ITSIM require knowledge of the multipole coefficients for the electric potential inside the ion trap that is being evaluated. For this study, the ion optical program SIMION 7.0 [23,24] was used to calculate these multipole coefficients in the following manner. A geometry file was created for a CIT to be modeled. The geometry file was imported into SIMION, the ring electrode potential was adjusted to +1 V and both endplates were grounded (0 V). An electron was “flown” through the center of the trap along the z -axis ($r=0$). The potential was recorded at equal step intervals by using the marker step function. The array of (z -position, electric potential) values was then imported into MATLAB 6.0 [25] and a least-squares fit (LSQF) of the nominally quadratic electric potential on the z -axis was performed to obtain the higher-order multipole coefficients of the electric potential. Determination of the multipoles with the least-squares fit in MATLAB 6.0 was performed to a polynomial with up to 44 poles to obtain the desired degree of accuracy for the lower order multipoles.

To validate the method to obtain multipole coefficients, SIMION was used to calculate the electric potential of an “idealized” CIT (i.e., one that has no endplate spacing and no endplate apertures) with $z_0/r_0 = 0.9$. The calculated values were then com-

Table 1

Comparison of multipole components of an “ideal” CIT ($z_0/r_0 = 0.9$, no apertures or endplate spacing) determined analytically and using the least-squares fitting method described in this work

Multipole number	Analytical multipole	Calculated multipole
A2	−0.848387	−0.848364
A4	−0.072415	−0.072439
A6	0.182100	0.182070
A8	−0.003054	−0.003010

pared with the analytical values calculated from Eq. (1),

$$A_{2n}^R = -\frac{2}{(2n)!} \cdot \sum_{i=1}^{\infty} \frac{x_i^{2n-1}}{\cosh((z_0/r_0)x_i)J_i(x_i)} + \delta_{n,0} \quad (1)$$

where J_0 and J_1 are the Bessel functions of the first kind, x_i is the i -th zero of $J_0(x)$ [22,26]. A minimum number of 1000 grid units along the z -axis between the CIT endplates was required in SIMION to obtain the same multipole coefficients from the least-squares fit using MATLAB as from Eq. (1) (see Table 1).

As an additional confirmation, the method was also used to calculate and compare previously published multipole components of CIT geometries with endplate apertures and endplate spacing [17]. The results are depicted in Table 2. The choice of polarity for sets of multipole coefficients is not consistent in the mass spectrometry literature and is arbitrary unless the phase of the RF voltage is being considered. The convention for this work was chosen to be consistent with the results in Table 1 (obtained from Eq. (1)) and are consequently of opposite polarity to the results of Wu et al. [17].

Multipole coefficients were then obtained by similar methods for the LTCC CIT constructed in this work. The dimensions of the LTCC CIT were based on previous unpublished work in this laboratory and are listed below using the terminology defined by Wu et al. [17] (see Fig. 1).

The CIT radius (r_0) was 1.375 mm and the center to end cap distance (z_0) was 1.580 mm; apertures in the endplate electrodes (r_H) were 0.4125 mm in radius (30% of r_0) and the endplates had a thickness of 0.10 mm. The gap between the ring electrode and the endplate electrodes (d_s) was chosen to be 0.475 mm and the half cylinder thickness (z_b) was 1.105 mm. The radius at which the bases of the cylindrical electrode on each side of the LTCC structure were truncated (r_b) was 0.900 mm. Table 3 lists the calculated multipole coefficients for the LTCC CIT.

These multipole coefficients were then entered into ITSIM along with the dimensions of the LTCC CIT. A simulated CHCl₃ mass spectrum was generated by flying 2424 ions

Table 2

Comparison of multipole components of CIT 0 reported by Wu et al. [17] and those determined using the least-squares fitting method described in this work

Multipole number	Wu et al.	Calculated multipole
A2	0.736	−0.736 ^a
A4	0.055	−0.054
A6	−0.131	0.132

^a Note the inversed sign, the cylindrical electrode was defined as +1 V. The endplates were grounded.

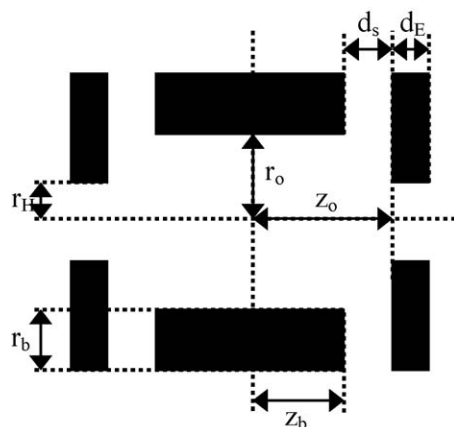


Fig. 1. Schematic to define the terminology used to describe the dimensions of CITs.

($m/z = 83$), 1557 ions ($m/z = 85$) and 250 ions ($m/z = 87$) – according to the expected isotope ratios of CHCl_2^+ – using the Langevin collision model with 1×10^{-4} Torr helium at a temperature of 300 K. The fourth-order Runge–Kutta integration step (2.5×10^{-9} s) was chosen to be at least 100 steps per RF cycle (2.5×10^{-7} s \cong 4 MHz) for the simulated experiments to ensure good precision. The ramp rate was set to 5 m/z per millisecond, which corresponded to 14 ms for one scan. The mass spectrum generated by ITSIM is shown along with experimental results in section 3 below.

2.2. Fabrication process

The fabrication of the LTCC ring electrode [27] was divided into five major steps as outlined by the flow diagram in Fig. 2. These steps, punching, lamination, firing, metallization and photolithography on the metallized layer, are discussed in detail in the following sections. Completion of the CIT construction required addition of stainless steel endplates, which is also discussed below.

2.2.1. Punching and lamination

LTCC sheets (951 Green TapeTM) from Dupont were used for fabrication of the structure. The thickness of each sheet was 0.1 mm. The sheets were cut using a punch designed taking both the CIT design and lateral shrinkage of the tape upon firing into account. Initially, the punch was designed to cut rings with a 19 mm outer diameter and 3 mm inner diameter. To ensure minimal distortion, the rings were cut in a single step using an assembly of concentrically aligned hammer punches. These circular sheets were stacked in a stainless steel die assembly (with

Table 3
Multipole components for the LTCC CIT determined using the least-squares fitting method described in this work

Multipole number	LSQF multipole
A2	−0.7349
A4	−0.1739
A6	0.2060

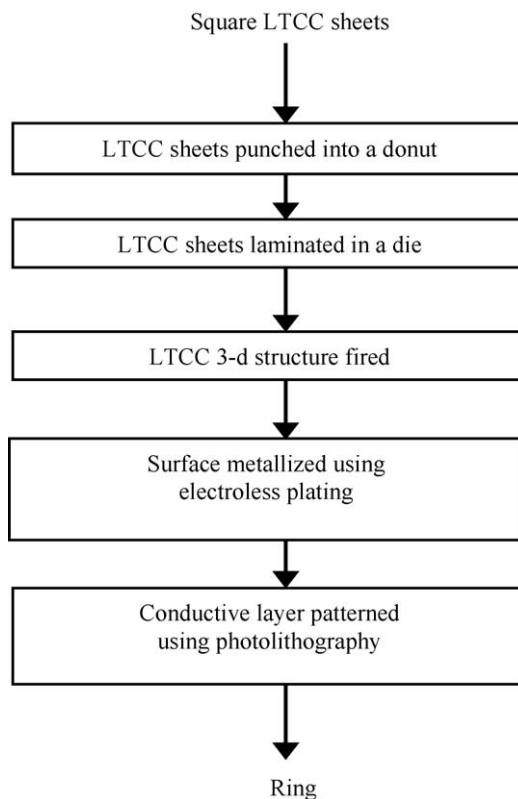
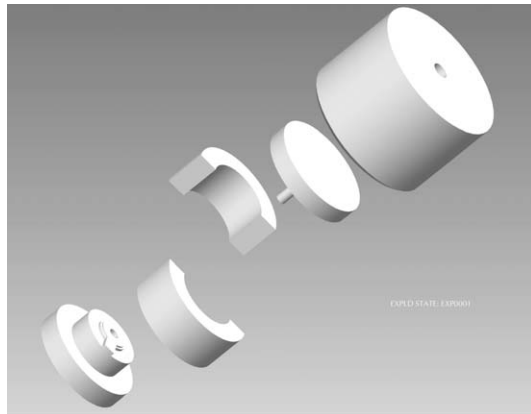


Fig. 2. Flow diagram for fabrication of the LTCC CIT.

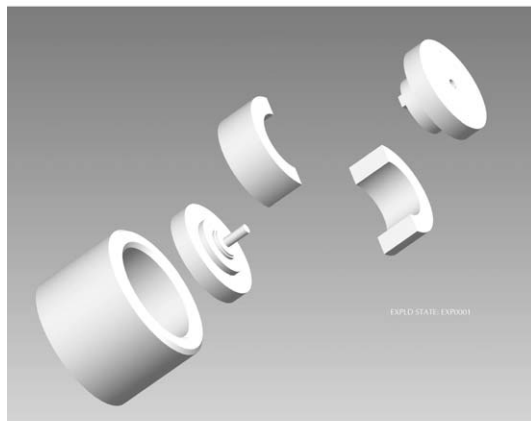
the inverse shape of the ring electrode) that was designed for lamination of the LTCC sheets. The results (structural integrity) were used to redesign the punch to yield two sets of doughnut shaped discs, one with an internal diameter of 3 mm (d_1) and the other with an internal diameter of 9.5 mm (d_2).

The die assembly, shown in Fig. 3, incorporated two concentric circular steps to transfer impressions on both sides of the soft LTCC structure; the first step was to provide the separation of the endplates from the ring electrode (required to prevent electrical short), and the second step was matched to fit and align the stainless steel endplates. Fig. 4 shows schematically the concentric steps in detail. Next the discs were assembled in a die such that 28 discs of diameter d_1 were sandwiched between 24 discs of diameter d_2 (12 on each side). The sheets were pressed in the die under 8000 psi at 85 °C for 15 min in a PHI P215H Hydraulic Lamination Press. These lamination parameters were found to be optimal for the die design through a series of previous experiments.

The final thickness of the laminated structure was defined by the die design. The number of sheets used and the lamination pressure were interdependent since the volume of the die was constant. For 52 LTCC sheets, the optimum compression was 8000 psi, which resulted in a semi-hard LTCC ring electrode with the patterns of the die transferred on it. After lamination and before firing, three holes were drilled in the LTCC ring electrode to allow for screws to hold the electrical connections in the final device. A channel was also incorporated into the 3D-structure for the purpose of electroless plating at a later stage to provide a connection for the RF high voltage to the ring electrode.

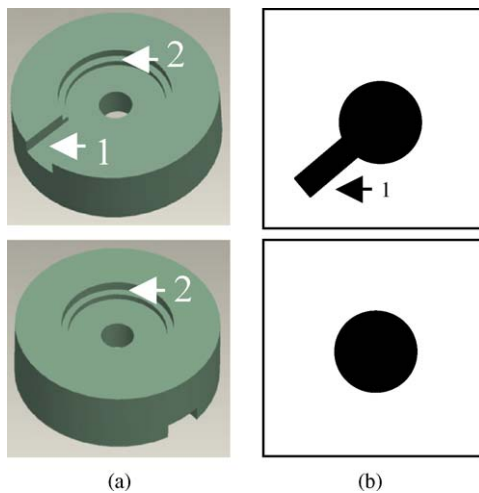


(a)



(b)

Fig. 3. Exploded 3D views of the stainless steel die assembly used for lamination: (a) view of the front side disc of the die with the inverse channel and (b) view of the backside disc of the die.



(a)

(b)

Fig. 4. 3D model of LTCC CIT ring electrode and schematic of mask used for patterning of the conductive layers: (a) top and bottom views of LTCC ring electrode and (b) corresponding areas for metallization. The channel in the top view is for electrical connection to the high voltage RF supply.

2.2.2. High-temperature firing

The soft LTCC ring electrode was fired in a Barnstead Thermolyne 21100 tube furnace at atmospheric pressure. The temperature was ramped to 350 °C at 10 °C/min where it was held constant for 30 min. At this temperature the LTCC lost all of its organic components [16,28]. The temperature was then increased at the same ramp rate to 850 °C, where it was held for 30 min. The glass transition temperature of the ceramic coat used in LTCC is 810 and at 850 °C the glass reflows and surrounds the grains of ceramic, forming a hard ceramic structure [16,28]. The resulting hard ceramic 3D-structure was allowed to slowly cool to room temperature.

2.2.3. Metallization and photolithography

Fig. 5 shows the steps taken to metallize and pattern the LTCC.

Step a and b: The entire LTCC ring electrode was plated with electroless Ni and then with Au to form a conductive surface. Electroless plating is an autocatalytic process that results in reduction of metal from the solution onto the immersed surface. This technique enables conformal coating of metals on non-conducting three-dimensional surfaces. The metallized surface is then used as a plating base for electro- or electroless plating of the desired metals. This two-step process ensures minimal stress in the plated films. Ni has excellent adhesion to the glassy surface of the ring electrode, and served as a seed layer on which gold was electroless plated. A Ni film, high in phosphorus, was used to eliminate the ferromagnetic behavior of Ni. Electroless Au was plated on top of the Ni to ensure a highly conductive layer, not prone to heating. The electroless Ni and Au were plated for 6 and 10 min, respectively, to get a 2.5 μm thick conductive layer for operation at RF high voltages (up to 1.5 kV_{0p} and 5.5 MHz in vacuum). The metal layers were then lithographically patterned and etched, as described below, in order to define the conducting and non-conducting regions.

Step c: Double sided mounting tape was used to attach the ring electrode structure onto a glass slide. The glass slide was then held by vacuum on the spinner chuck. Positive photoresist (Shipley 1827) was spun onto the LTCC structure at 2500 rpm

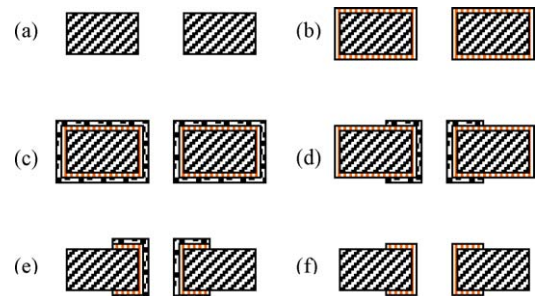


Fig. 5. Process flow for patterning of conductive metal layer on the surface of the LTCC ring electrode: (a) bare LTCC electrode substrate; (b) substrate plated with electroless Ni and Au; (c) positive photoresist spun onto both sides; (d) photoresist patterned using maskless photolithography [29]; (e) metal layer stripped in selected areas; (f) remaining photoresist stripped.

for 30 s. Since there was a hole at the center of the ring electrode, photoresist was spun on both sides of the LTCC structure in one spinning operation. The substrate was removed from the glass slide, placed on another glass slide and soft baked at 120 °C for 60 s. Next the photoresist was exposed by using a SF100 [29]; a direct write lithography tool. In this machine, a computer-generated mask was directly imposed via Digital Light Processing™ (DLP) projection of UV light of 488 nm on the 3D-structure. The LTCC structure was manually aligned on an X–Y–Z stage with the projection of the mask (using 570 nm light) from the SF100 and was then exposed with UV light of 488 nm for 8 s. The mask, shown in Fig. 4, defined the area where the photoresist was exposed, and therefore those areas where metal was to be removed.

Step d: The UV-exposed portion of the photoresist was developed and removed with Microposit™ 453 developer. The resist was developed for 45 s. Similar steps were followed on the other side to pattern the photoresist on the backside with the backside mask (Fig. 4).

Step e: Once the photoresist was patterned and developed the LTCC structure was dipped 7 min in aqua regia (HCL:HNO₃::3:1) solution to remove the exposed metal layers. Aqua regia stripped the metal layers except at those regions that were protected by the patterned photoresist layer.

Step f: The obtained LTCC structure was cleaned in acetone and methanol to dissolve all photoresist residues and was baked at 85 °C to remove any volatile compounds present.

2.2.4. Assembly of CIT

Stainless steel endplate electrodes with an aperture of 0.42 mm radius and a thickness of 0.10 mm were then fitted in the circular grooves on each side of the LTCC ring electrode to complete the CIT, as shown in Fig. 6. Tab washers constructed from stainless steel sheet held the endplate electrodes in the grooves. The CIT was attached to a stainless steel plate for mounting in the vacuum system. The conductive channel in the LTCC ring electrode was electrically connected to the plate by a copper strip for application of the RF high voltage.

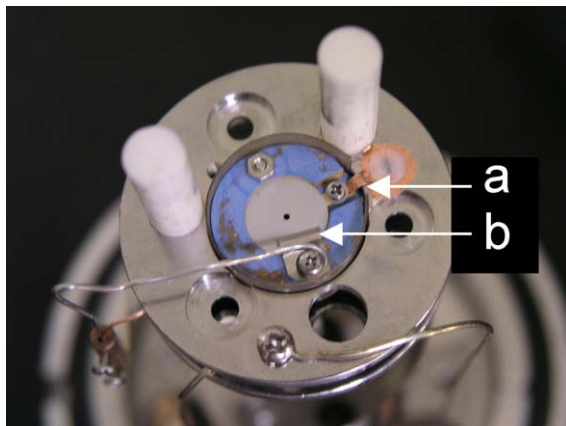


Fig. 6. Photograph of LTCC CIT assembly mounted on a vacuum flange: (a) a copper strip connected to the conductive channel on the LTCC ring electrode and (b) endplate electrodes secured to LTCC ring electrode using a tab washer.

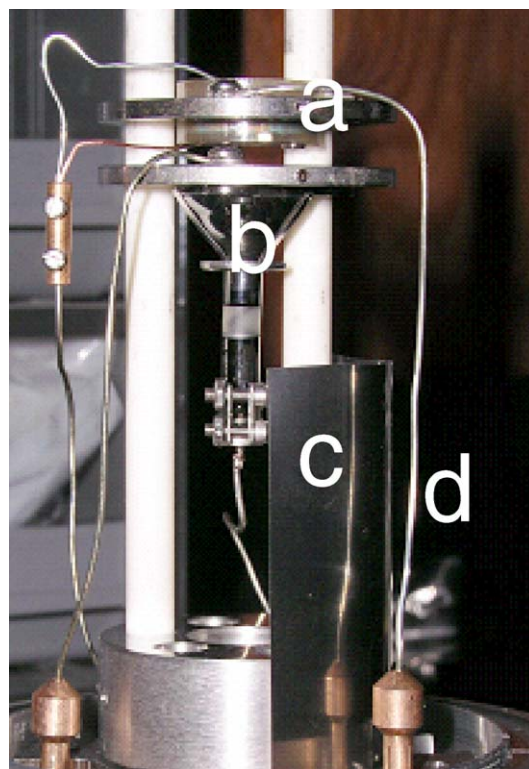


Fig. 7. Photograph of the CIT assembly and detector mounted on a vacuum flange: (a) LTCC CIT; (b) electron multiplier detector; (c) stainless steel RF shield; (d) RF high voltage lead.

2.3. Experimental test setup

The CIT assembly was mounted onto a vacuum flange that was fitted with a series of electrical feedthroughs (see Fig. 7). An electron multiplier detector (DeTech XP-2074) was mounted next to one aperture of the CIT. The RF high voltage electrical connection from the flange feedthrough to the ring electrode was shielded from the detector with a stainless steel sheet to avoid pick up of the RF high voltage. The CIT endplate electrodes were grounded to the vacuum flange. The vacuum flange was mounted on a vacuum chamber that had two separate gas inlets, one for analytes and the other for a buffer gas. An electron gun (Kimball Physics Inc. ELG-2/EGPS-2) was used for ionization of the analytes. When mounting the CIT the front side of the electron gun was automatically aligned at a distance of 2 cm from the CIT aperture. Fig. 8 shows a detailed diagram of the experimental setup.

To obtain the correct RF voltages and ramp rates a Stanford DG535 digital delay/pulse generator was used to gate the electron beam for ionization, reduce the detector high voltage during ionization and start and stop the RF ramp for mass analysis. A Wavetek Datron 195 waveform generator was used to provide a sinusoidal voltage that was ramped in amplitude after an ionization period of 50 ms. This signal was amplified by an ordinary broadband AB push/pull amplifier to generate a high current signal. The output of the broadband amplifier was directly coupled with an inductor that was attached to the CIT. This combination gave a series resonant circuit in which current was transformed

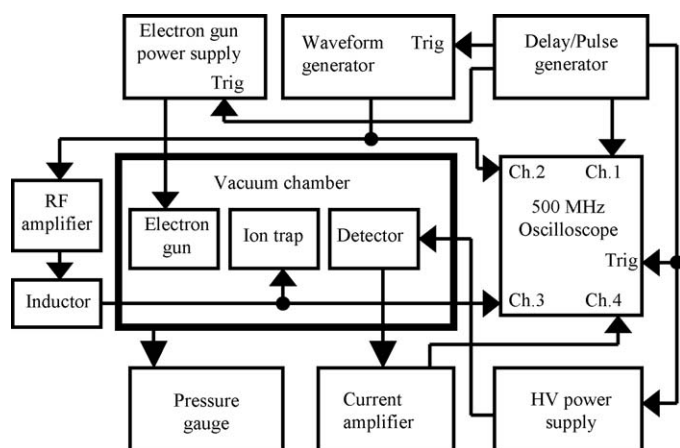


Fig. 8. Block diagram of the experimental test setup.

to high voltage. To change the resonant frequency the inductance of the circuit was changed. The frequency of the waveform generator was adjusted to obtain a linear ramp. The average power absorbed by the broadband amplifier was about 2–3 W. During ionization the RF trapping voltage (CHCl_3 at 3.926 MHz, PFTBA at 2.970 MHz) was set at $114 V_{0p}$. Then the electron gun was switched off and the RF trapping voltage was ramped from 114 to $770 V_{0p}$ in 20 ms. The detector voltage was switched with a KEPCO high voltage power supply by the Stanford digital delay/pulse generator. The detector was held at -1600 V during the ramping and was held at -1000 V during electron ionization to protect against excessive current from ions created in front of the detector.

The LTCC CIT was tested in the mass selective instability mode using PFTBA (calibration gas) and CHCl_3 as analytes, and helium as a buffer gas. The analytes were leaked into the vacuum chamber and were ionized by the electron beam from the electron gun that was operated at 77 eV. The RF voltage amplitude was ramped to eject ions in ascending order of m/z . The ions that impinged on the detector generated a signal current that was amplified with a current amplifier (Advanced Research Instruments Co. PMT5) at a gain of 10^6 V/A . The signal current was visualized with a LeCroy 9354A oscilloscope to obtain a plot of ion intensity versus time. The RF voltage amplitude of the ramp was recorded for all the instances and the spectrum was corrected with respect to m/z .

3. Results and discussion

3.1. Fabrication processes

In the fabrication process the optimum lamination pressure range was found to be higher than that used in the typical LTCC lamination for high-density electronic packing. Initial experiments showed that stresses in the laminated LTCC structure during firing caused cracks in the center of the ring electrode. To reduce stresses and avoid cracks in successive experiments the LTCC sheets were cut in different shapes, then stacked and laminated. The shaping was done to ensure uniform pressure loading in the die relief, as seen in Fig. 9. Fig. 9a schematically

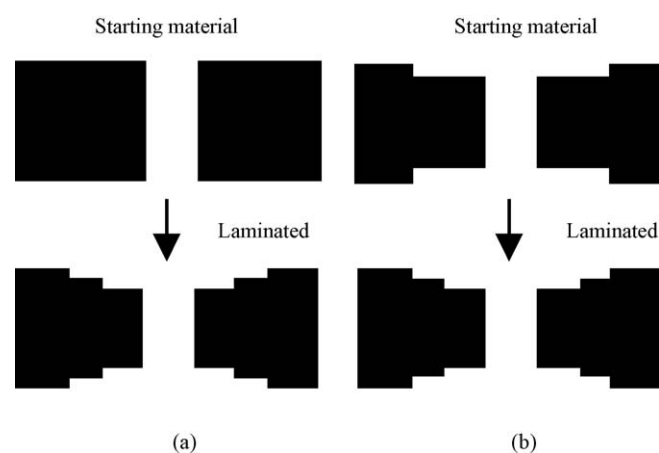


Fig. 9. Representations of cross sectional views of LTCC sheets in the stainless steel die during lamination: (a) non-uniform compression of 52 sheets and (b) uniform compression: 28 sheets of LTCC with a smaller inner diameter ($d_1 = 3 \text{ mm}$) were used in the center region and 12 sheets with a larger inner diameter ($d_2 = 9.5 \text{ mm}$) in the outer regions ($12 + 28 + 12$).

shows the result of pressing a stack of laminated sheets into a three dimensional profile. This approach was used in the first set of experiments. In this approach, the green tapes at the center need to be pressed the most, resulting in non-uniform compacting and cracking. As discussed above, the process was modified by shaping the starting material to be close to its final profile as shown in Fig. 9b. This approach results in more uniform compression and eliminates cracking.

Also, the design of the stainless steel die assembly was modified in order to achieve a relatively uniform compression of the material throughout the die volume. The shrinkage during the firing process was found to be smaller because the material was more tightly packed as a result of the higher lamination pressure. Experiments were conducted to optimize the number of sheets used in the lamination process so that shrinkage during the firing process was repeatable and could be compensated for in the design. Once the trap was fabricated, its final dimensions were recorded to calculate the post firing shrinkage. The percentage of post-firing shrinkage was found to be $10 \pm 0.5\%$ in the X–Y direction and $9.5\% \pm 0.5\%$ in the Z-direction. The overall tolerance of 1% found in this process can be improved by at least one order of magnitude by fabricating the ion traps in standard processing plants and using improved metrology tools. This is routinely achieved in manufacturing as variables (pressure, temperature and humidity) are better controlled. The 1% precision in the current manufacturing process for either r_0 or z_0 translates into a shift of the mass spectra by less than one mass unit. The concept of using a die assembly to obtain 3D structures could allow for batch fabrication; by incorporating multiple die units in one and lamination of an entire stack of LTCC sheets at one time. This could be an inexpensive alternative to the conventional method of building CIT mass spectrometers of stainless steel. It can be very crucial in simplifying the complex ion optic assemblies and the alignment issues. The provision for auto-alignment of different components with the help of grooves and protrusion geometries can make the overall assembly simple.

Table 4
Experimental parameters for tests of the LTCC CIT

Total pulse sequence	120 ms
El time	50 ms
Ramp time	20 ms
Frequency of RF signal	2.79 MHz
Starting voltage	114 V
Final voltage of ramp	770 V
Gain of current ampere	1×10^6 V/A
Temperature	25 °C
Electron energy	77 eV
Detector power supply	–1600/–1000 V
PFTBA pressure	0.9×10^{-6} Torr
PFTBA + He pressure	1.0×10^{-3} Torr
Background pressure	1.3×10^{-6} Torr
CHCl ₃ pressure	1.8×10^{-5} Torr
CHCl ₃ + He pressure	1.0×10^{-3} Torr
Background pressure	4.3×10^{-7} Torr

The approach of selective metallization of a non-conductive 3D substrate using photolithography has its advantages, which are derived from the precision of the photolithography technique. A tighter tolerance of the metal layer can allow for better control over the electric potential inside the CIT and hence its characteristics. Initially two different photolithographic methods were tried; one with a positive and, the other with a negative photoresist. The method with negative photoresist (PKP) was discarded, as the PKP was hard to strip after development.

3.2. Simulation and experimental tests

Table 4 shows details of the experimental parameters used to obtain mass spectra of PFTBA and CHCl₃. Pressures reported were uncorrected. Although the characteristic fragment ions of PFTBA corresponding to m/z 69, 100, 131, 169, and 219 were easily identified, a typical but significant background signal was present due to initial outgassing of the vacuum chamber and the LTCC structure, see Fig. 10. The CIT performed well with PFTBA present at 1×10^{-6} Torr. Helium buffer gas improved

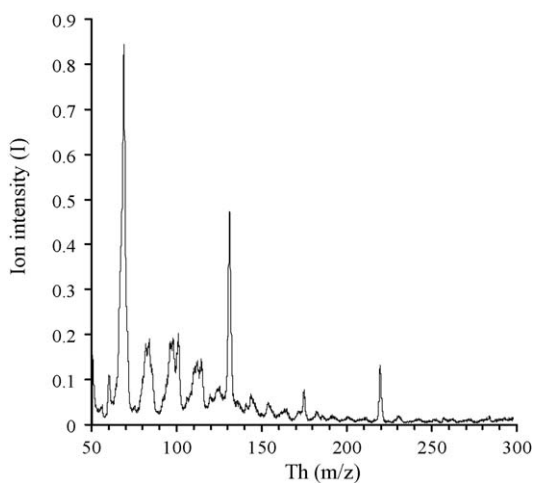


Fig. 10. A mass spectrum of PFTBA (0.9×10^{-6} Torr) obtained from the LTCC CIT Helium was used as a buffer gas (1×10^{-3} Torr) and the RF frequency was 2.970 MHz.

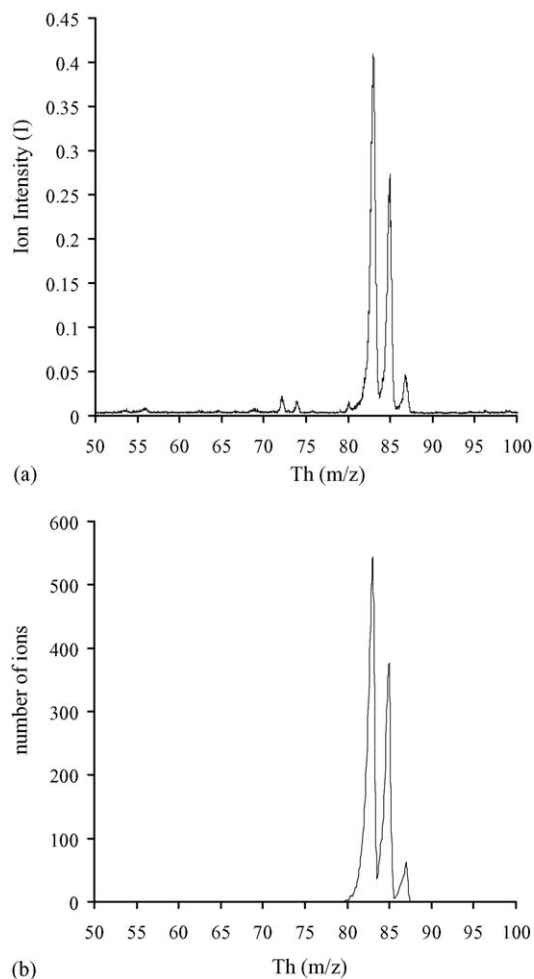


Fig. 11. Mass spectra of CHCl₃ obtained by experiment and simulations: (a) a mass spectrum of CHCl₃ (1.8×10^{-5} Torr) obtained from the LTCC CIT. Helium was used as a buffer gas (1×10^{-3} Torr) and the RF frequency was 3.926 MHz and (b) simulated mass spectrum of CHCl₂⁺ fragment of CHCl₃ obtained from ITSIM using geometrical parameters of the LTCC CIT.

the resolution to 1.8 m/z determined with the full width at half maximum (FWHM) method.

The mass spectrum recorded with CHCl₃ present in the chamber shows clearly the isotopic pattern of CHCl₂⁺ (see Fig. 11a). The lower background signal indicated that the initial outgassing was diminished. The mass spectrum obtained from the simulations in ITSIM is shown in Fig. 11b and is remarkably similar to the mass spectrum of CHCl₃ obtained during the experiments.

4. Conclusions

A miniature CIT mass spectrometer was constructed using a non-conductive substrate (LTCC) as the basis for the ring electrode. Photolithography and electroless plating were used to create well-defined conductive areas on the LTCC ring electrode. After adding stainless steel aperture plates, the LTCC CIT was successfully tested using PFTBA and CHCl₃ as analytes and helium as the buffer gas. The mass spectra obtained had a typical peak width of 1.8 m/z (FWHM). Higher-order multipole contributions to the potential inside the CIT were determined with

SIMION and were used for simulations in ITSIM to confirm operation. Use of soft materials, such as LTCC, could possibly lead to batch fabrication strategies for miniature arrays of cylindrical ion trap mass spectrometers. Precise control over the placement of conductive areas on LTCC might also be useful for new types of electrodes in ion optical systems.

Acknowledgements

This work was supported by the US SMDC, under contract DASG60-00-C-0089. The authors also wish to thank R.G. Cooks for providing ITSIM.

References

- [1] C.R. Arkin, T.P. Griffin, J.A. Diaz, D.W. Follistein, C.H. Curley, D.P. Floyd, G.R. Naylor, W.D. Haskell, M. Blalock, F.W. Adams, *Trends Anal. Chem.* 23 (2004) 322.
- [2] P.G. Wenner, R.J. Bell, F.H.W. van Amerom, S.K. Toler, J.E. Edkins, M.L. Hall, K. Koehn, R.T. Short, R.H. Byrne, *Trends Anal. Chem.* 23 (2004) 288.
- [3] A.S. Creba, R.M. Ferguson, A.J. Thompson, R.L. Dills, C.D. Simpson, E.T. Krogh, C.G. Gill, *Proceedings of the 53rd ASMS Conference on Mass Spectrometry and Allied Topics*, San Antonio, TX, 2005.
- [4] G.E. Patterson, A.J. Guymon, L.S. Riter, M. Everly, J. Griep-raming, B. Laughlin, Z. Ouyang, R.G. Cooks, *Anal. Chem.* 74 (2002) 6145.
- [5] E.R. Badman, R.G. Cooks, *Anal. Chem.* 72 (2000) 5079.
- [6] A. Tabert, J. Griep-Raming, A.J. Guymon, R.G. Cooks, *Anal. Chem.* 75 (2003) 5656.
- [7] E.R. Badman, R.G. Cooks, *J. Mass Spectrom.* 35 (2000) 659.
- [8] W.B. Whitten, P.T.A. Reilly, J.M. Ramsey, *Rapid Commun. Mass Spectrom.* 18 (2004) 1749.
- [9] O. Kornienko, P.T.A. Reilly, W.B. Whitten, J.M. Ramsey, *Anal. Chem.* 72 (2000) 559.
- [10] M.J. Madsen, W.K. Hensinger, D. Stick, J.A. Rabchuk, C. Monroe, *Appl. Phys. B* 78 (2004) 639.
- [11] S. Boumsellek, R.J. Ferran, *J. Am. Soc. Mass Spectrom.* 12 (2001) 633.
- [12] M.G. Blain, L.S. Riter, D. Cruz, D.E. Austin, G. Wu, W.R. Plass, R.G. Cooks, *Int. J. Mass Spectrom.* 236 (2004) 91.
- [13] E.R. Badman, R.G. Cooks, *Anal. Chem.* 72 (2000) 3291.
- [14] H. Kopola, J. Lenkkeri, K. Kautio, A. Torkkeli, O. Rusanen, T. Jaakola, *Proc. SPIE* 4592 (2001) 148.
- [15] K. Kordás, A.E. Pap, J. Saavalainen, H. Jantunen, P. Moilanen, E. Haapaniemi, S. Leppävuori, *IEEE Trans. Adv. Packag.* 28 (2005) 259.
- [16] K. Vaed, J. Florkey, S.A. Akbar, M.J. Madou, J.J. Lannutti, S.S. Cahill, *J. Microelectromech. Syst.* 13 (2004) 514.
- [17] G. Wu, R.G. Cooks, Z. Ouyang, *Int. J. Mass Spectrom.* 241 (2005) 119.
- [18] C.R. Arkin, B. Goolby, D.A. Laude, *Int. J. Mass Spectrom.* 190/191 (1999) 47.
- [19] E.C. Beaty, *Phys. Rev. A* 33 (1986) 3645.
- [20] J.M. Wells, E.R. Badman, R.G. Cooks, *Anal. Chem.* 70 (1998) 438.
- [21] J. Franzen, *Int. J. Mass Spectrom. Ion Processes* 125 (1993) 165.
- [22] W.R. Plass, Ph.D. Thesis, Justus-Liebig-Universität Giessen, Germany, 2001.
- [23] M.W. Forbes, M. Sharifi, T. Croley, Z. Lausevic, R.E. March, *J. Mass Spectrom.* 34 (1999) 1219.
- [24] D.A. Dahl, *Int. J. Mass Spectrom.* 200 (2003) 3.
- [25] The Mathworks, Inc., 3 Apple Hill Drive, Natick, MA 01760-2098, USA.
- [26] O. Kornienko, P.T.A. Reilly, W.B. Whitten, J.M. Ramsey, *Rapid Commun. Mass Spectrom.* 13 (1999) 50.
- [27] A. Chaudhary, F.H.W. van Amerom, S. Bhansali, R.T. Short, *Tech. Proc. 2004 NSTI Nanotechnology Conference and Trade Show*, vol. 1, MEMS Design and Application, 2004, p. 371 (Chapter 8).
- [28] Dupont Microcircuit Materials, 951 Green Tape Thick Film Composition, Product datasheet MCM951(1/03), Dupont.
- [29] Application Note: 010803 SF-100 Processing Capabilities, Intelligent Micropatterning LLC.